NANO LETTERS

pubs.acs.org/NanoLett

Letter

Revealing Variable Dependences in Hexagonal Boron Nitride Synthesis via Machine Learning

Ji-Hoon Park, Ang-Yu Lu, Mohammad Mahdi Tavakoli, Na Yeon Kim, Ming-Hui Chiu, Hongwei Liu, Tianyi Zhang, Zhien Wang, Jiangtao Wang, Luiz Gustavo Pimenta Martins, Zhengtang Luo, Miaofang Chi, Jianwei Miao, and Jing Kong*

Cite This: *Nano Lett.* 2023, 23, 4741−4748

Read Online

ACCESS | Metrics & More | Article Recommendations | Supporting Information

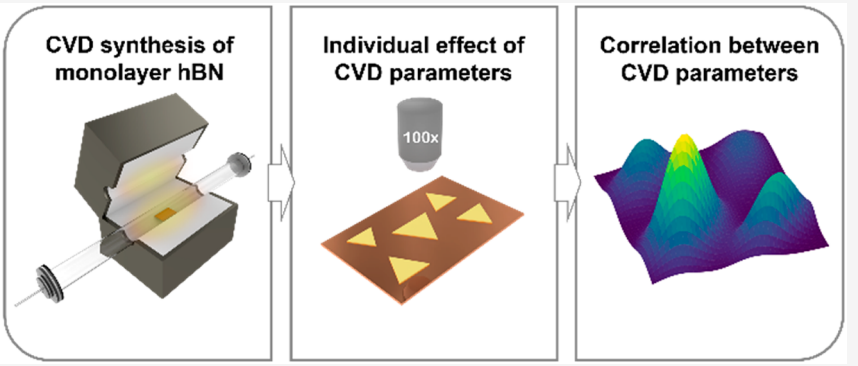

ABSTRACT: Wafer-scale monolayer two-dimensional (2D) materials have been realized by epitaxial chemical vapor deposition (CVD) in recent years. To scale up the synthesis of 2D materials, a systematic analysis of how the growth dynamics depend on the growth parameters is essential to unravel its mechanisms. However, the studies of CVD-grown 2D materials mostly adopted the control variate method and considered each parameter as an independent variable, which is not comprehensive for 2D materials growth optimization. Herein, we synthesized a representative 2D material, monolayer hexagonal boron nitride (hBN), on single-crystalline Cu (111) by epitaxial chemical vapor deposition and varied the growth parameters to regulate the hBN domain sizes. Furthermore, we explored the correlation between two growth parameters and provided the growth windows for large flake sizes by the Gaussian process. This new analysis approach based on machine learning provides a more comprehensive understanding of the growth mechanism for 2D materials.

KEYWORDS: *hexagonal boron nitride, chemical vapor deposition, growth parameter, machine learning, Gaussian process*

Monolayer hexagonal boron nitride (hBN), a member of the two-dimensional (2D) material's family, is the thinnest insulator, exhibiting a bandgap of ∼6 eV.[1] Owing to its atomic thickness as well as chemical and thermal stability, monolayer hBN has been extensively investigated for diverse applications, from membrane to catalyst.[2−5] Among the different synthesis approaches, chemical vapor deposition (CVD) is the most extensively used method for synthesizing large-area and high-quality monolayer hBN. To improve hBN crystallinity, researchers have focused on preparing single-crystalline metal substrates to grow single-crystalline monolayer hBN.[6−10] Although wafer-scale single-crystal monolayer hBN has been synthesized via this method, the study of the CVD growth dynamics of monolayer hBN, especially its dependence on the growth parameters, remains elusive. One of the reasons is the high adsorption energy of the B−N pair in hBN on the metal surface, leading to a high nucleation density and small grain sizes, making it difficult to keep track of the growth trend of hBN.[11,12] Therefore, the control of the nucleation density and the flake size of monolayer hBN is paramount to elucidate its growth mechanism for a given set of growth parameters.

The synthesis optimization of hBN is a multivariational problem involving several growth parameters such as the growth temperature, the type of substrate, precursor, carrier gas, etc. Each growth parameter not only affects the quality and properties of hBN, such as its morphology, growth rate, flake size, and thickness,[13−15] but also has synergies, leading to a black-box scenario. For example, the growth temperature can

Received: November 23, 2022
Revised: May 12, 2023
Published: May 17, 2023

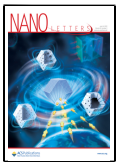

https://doi.org/10.1021/acs.nanolett.2c04624
Nano Lett. 2023, 23, 4741−4748

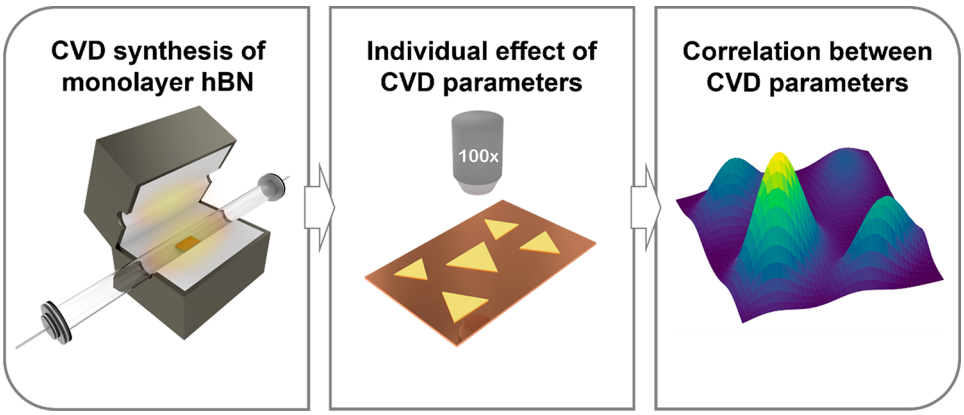

Figure 1. Schematic diagram of the analysis process. Step 1: monolayer hBN growth on single-crystalline Cu (111). Cu (111) was prepared via the converting process from polycrystalline Cu foil, and the nucleation density of hBN is influenced by borazine concentration. Step 2: individual effect of CVD parameters for hBN growth. CVD parameters such as the growth temperature, the flow rate of the carrier gas, and the concentration of the precursor were tuned individually during the growth process to observe the variation of lateral flake size and nucleation density of hBN. Step 3: understanding of the correlation between CVD parameters via Gaussian process regression. The Matérn kernel (eq 1) is used as a kernel function in the Gaussian process.

change the decomposition rate and the concentration of precursors as well as the desorption and diffusion of precursor species on metal substrates during the growth process.[16] In this context, a systematic understanding of the effect of these parameters on the hBN growth is crucial for a clear explanation of the growth mechanism and the synthesis of the desired outcome, including the quality and reproducibility of monolayer hBN growth. However, most studies have focused on the individual effects of the growth parameters for hBN synthesis due to the limited resources for analyzing the experimental data. Furthermore, the complex correlations between the parameters make it difficult to use traditional computation approaches based on atomic modeling simulations, such as density functional theory (DFT) and molecular dynamics (MD).[11,17] In the past decade, machine learning (ML) techniques have become a popular tool to unravel hidden patterns (black-box function) from nonlinear data sets using an approximate or surrogate model while requiring lower computational costs. For example, Gaussian processes (GP) are an efficient surrogate model for black-box functions because of their flexibility and ability to estimate uncertainties.[18] This nonlinear and nonparametric regression tool considers the covariance matrix between experimental input values via kernel function in GP and then interpolates the unknown data points scattered in multidimensional input space to predict mean and variance functions in the black-box function.

In this work, we synthesize monolayer hBN on single-crystalline Cu (111) substrates via low-pressure CVD. The nucleation density and flake size of hBN are controlled by the concentration and flow rate of the precursor, borazine, during the growth process. Furthermore, we systematically investigate the growth effects from single parameters to two parameters by the GP, allowing us to explore the correlation between the growth parameters. The result shows that borazine is the most sensitive parameter in our experiments by quantifying the correlated strength. Also, the growth temperature shows a strong correlation with hydrogen and borazine flow rates due to chemical reactions. This approach not only reveals the effects of various growth parameters and their correlations for the hBN synthesis but should also open new insights for the systematic understanding of the growth mechanism of related 2D materials.

Figure 1 shows the simple flowchart of this work, which includes three steps. The first step is the synthesis of monolayer hBN on single-crystalline Cu (111). Because the catalytic activity of Cu is dominated by its grain orientation, we converted commercial polycrystalline Cu into single-crystalline Cu (111) via a contact-free annealing process (Supporting Information, Figure S1 and Experimental Section).[7] Then, the single-crystalline Cu (111) foils are used as the growth substrates, providing a smooth and grain boundary-free surface for high-quality monolayer hBN growth. The Cu (111) foils are placed between an alumina and a sapphire plate, forming a sandwich structure to reduce the nucleation density of hBN and Cu evaporation (Figures 2a and S2). To prepare the precursor for the hBN growth, we diluted liquid borazine ($B_3H_6N_3$) in argon gas in a home-built precursor chamber (Figure 2a). Afterward, we flowed the diluted borazine precursor, which was controlled using a mass flow controller (MFC). The second step is to unravel the individual effect of the CVD parameters on the hBN growth. We tuned only one growth parameter in a given synthesis, such as the growth temperature, the flow rate of the hydrogen gas, or the flow rate of borazine. Afterward, we measured the lateral flake size and nucleation density of hBN crystals on single-crystalline Cu (111) using an optical microscope. Based on these results, we analyzed the effects of individual parameters on the hBN growth. The last step is to understand the correlation between two parameters via an ML approach. In this process, GP is a surrogate model that builds the predicted black-box function, consisting of the mean and covariance functions through a stochastic process from past experimental input values. This considers the covariance matrix between input values via the kernel function in the GP model. Therefore, we focus on the GP that shows the covariance between input variables from a multidimensional perspective. Equation 1 shows the Matérn52 kernel as a kernel function in GP.[18]

$$K(x_i, x_j) = \left(1 + \frac{\sqrt{5}d}{l} + \frac{5d^2}{3l^2}\right)\exp\left(-\frac{\sqrt{5}d}{l}\right) \quad (1)$$

https://doi.org/10.1021/acs.nanolett.2c04624
Nano Lett. 2023, 23, 4741−4748

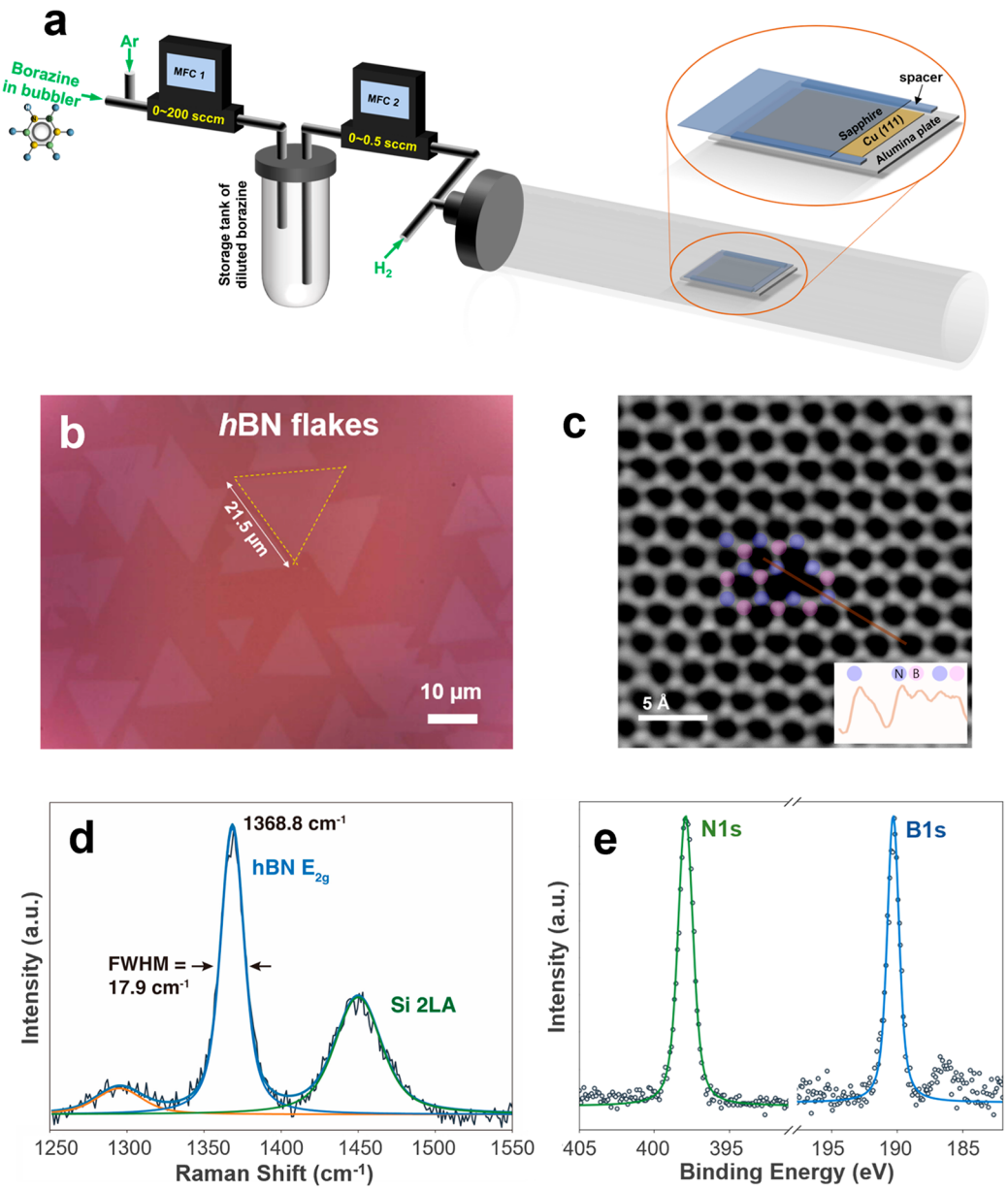

Figure 2. Monolayer hBN growth on Cu (111). (a) Schematic of the experimental setup of the CVD system for the hBN growth. (b) Triangle-shaped flakes of monolayer hBN grown on Cu (111). (c) High-resolution STEM image of hBN. Boron and nitrogen atoms are noted by the superposition of the ball (magenta ball: B; blue ball: N), and the intensity profile is plotted as a solid brown line. The atomic defect in the center of the image was induced by beam damage during the measurement. (d) Raman spectrum of transferred hBN on a SiO_2 substrate. The E_{2g} peak corresponding to the in-plane vibration of hBN is observed at the position of 1368.8 cm^{-1}, which ensures monolayer characteristics in the range from 1368 to 1370 cm^{-1}. (e) High-resolution XPS B 1s and N 1s peaks of an as-grown hBN on Cu (111).

where x_i and x_j are input points. d is the distance between two points (x_i and x_j), and l is a length scale parameter. The Matérn52 kernel is a stationary kernel that only depends on the distance of two data points and computes the similarity between two input points.

Figure 2b displays an optical image of monolayer hBN flakes grown on single-crystalline Cu (111) foil by low-pressure CVD. The hBN flakes exhibit triangular shapes with sizes up to 21.5 μm and well-aligned orientations, indicating their epitaxial growth on single-crystalline Cu (111) (Figure S1). Figure 2a shows schematics of the experimental setup of our CVD system for the hBN growth. Borazine was filled into the bubbler system and was stored at 0 °C by a cooler, which prevented its self-decomposition to polyborazylene.[19] Argon gas was used as a carrier gas to deliver borazine into the synthesis chamber. Compared to ammonia borane, which is another popular precursor for hBN growth, borazine exhibits a lower evaporation temperature and higher catalytic activity on metal substrates, leading to smaller flake sizes and higher nucleation densities. Therefore, we adopted a three-step process to dilute the concentration of borazine. The first step is a mixture process with pure argon gas in borazine. The argon flow rate was precisely controlled by the first MFC, and the mixture source was collected in a storage tank located between the bubbler and the quartz tube. The second step is the control process of the flow rate. The mixture source was precisely controlled by the second MFC within a maximum flow rate of 0.5 sccm and flowed to the quartz tube. The final

https://doi.org/10.1021/acs.nanolett.2c04624
Nano Lett. 2023, 23, 4741−4748

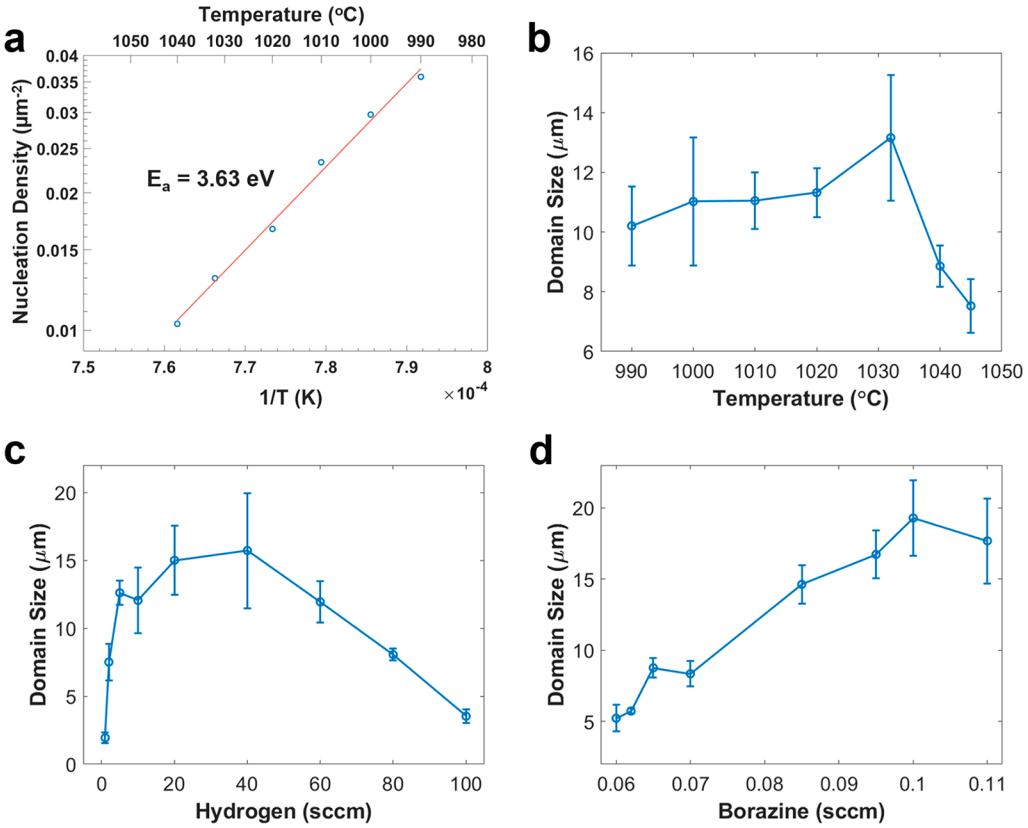

Figure 3. Individual effects of the CVD parameters on the hBN growth. (a) Arrhenius plot of the nucleation density of monolayer hBN at different growth temperatures. The nucleation densities of hBN monolayers at different temperatures are calculated from the optical microscopic images in Figure S5 and labeled as blue dots. The slope of the red line corresponds to the nucleation activation energy of 3.63 eV. (b−d) Plots of the lateral domain size of hBN as a function of the (b) growth temperature at a fixed borazine flow rate of 0.085 sccm and hydrogen flow rate of 40 sccm, (c) the hydrogen flow rate at a fixed growth temperature of 1030 °C and borazine flow rate of 0.085 sccm, and (d) the borazine flow rate at a fixed growth temperature of 1030 °C and hydrogen flow rate of 40 sccm (the melting point of Cu (111) foil in our system is 1047 °C).

step is to use a sandwich structure as a surface treatment of the substrate, in which a sapphire plate covers the Cu foil on the alumina plate. The gap between the Cu foil and the sapphire plate is controlled by spacers with an optimized gap height of 300 μm. The sandwich structure helps to obtain a smooth Cu surface due to the suppression of Cu evaporation and the increase of lateral diffusion of Cu atoms, as shown in Figure S2.[20,21] Therefore, the excess of hBN nucleation sites, such as defects and protrusions on the Cu surface, can be significantly reduced.

Figure 2c shows a high-resolution scanning transmission electron microscopy (STEM) image of the atomic lattice structure of hBN monolayers. Scanning electron microscopy (SEM) and atomic force microscopy (AFM) analysis (Figure S3) confirm the cleanliness of the surface and the thickness of the hBN. The AFM line profile indicates a thickness of 0.31 nm, as expected for monolayer hBN. This result is consistent with the Raman spectrum in Figure 2d.[22] As the growth time increases, the hBN flakes increase in size and merge into a continuous film, as shown in Figure S4. To confirm the atomic elements of hBN, we performed X-ray photoelectron spectroscopy (XPS). Figure 2e shows the B 1s and N 1s core-level peaks at 190.3 and 397.8 eV, respectively, obtained from an as-grown hBN film on Cu (111). The stoichiometry of B and N atoms is 1:1.09. These features indicate the good quality of the synthesized monolayer hBN.

Figure 3a shows the plot of the nucleation density as a linear function of the substrate temperature. The linear fitting shows an Arrhenius activation energy of 3.63 eV, indicating a higher energy barrier for the hBN molecules to adsorb on the copper surface compared with previous studies.[12,23] This has been attributed to the smoothness and catalytic properties of single-crystalline Cu compared to polycrystalline Cu, which exhibits a rough surface and higher surface energy (which correspond to lower energy barrier for the hBN molecules to absorb).[6,8] To understand the growth mechanism of hBN, we investigate the individual effects of various CVD parameters. Figure 3b shows the plot of the domain size as a function of the growth temperature in the range of 990 to 1045 °C. The domain size was obtained by choosing ten flakes with the largest sizes and calculating the average in each optical image (Figure S6). Under a fixed growth time of 20 min, the hBN flakes with triangular shape are mostly aligned on the Cu (111) (Figure S5b−e). At the growth temperature of 980 °C, hBN crystals form a continuous film with high nucleation density and small flake sizes in the whole area. The flake sizes of hBN slightly increases from 10.2 μm at 990 °C to 13.16 μm at 1030 °C with the same growth time. In that temperature range, the dissociation of the borazine adsorbed on the Cu surface is accelerated, leading to more B and N atoms or intermediate products such as polyborazylene. The mean free path of B and N atom diffusion increases as the growth temperature increases within this range.[13,24] However, the flake size of hBN decreases when the growth temperature increases above 1030 °C. There could be multiple reasons contributing to this observation, such as an increased dissolution of B atoms into the bulk of

https://doi.org/10.1021/acs.nanolett.2c04624
Nano Lett. 2023, 23, 4741−4748

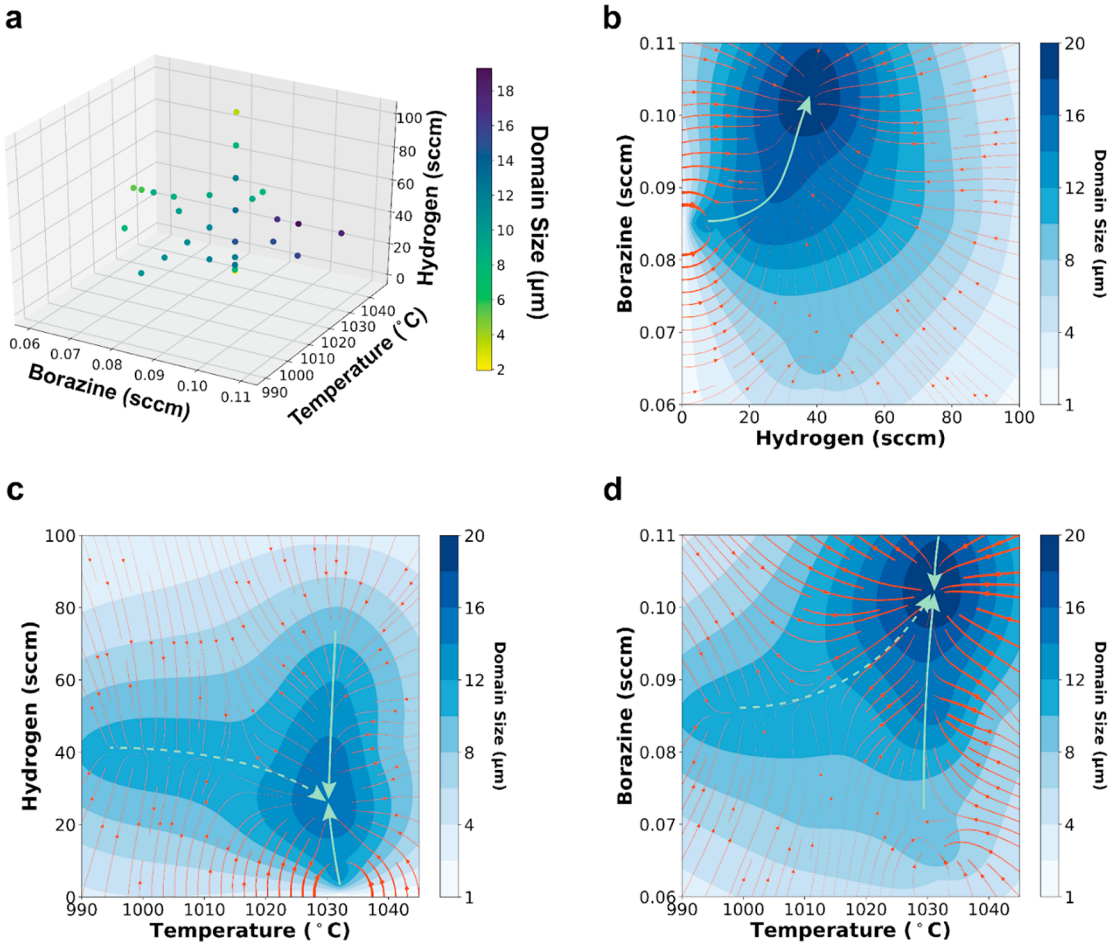

Figure 4. Gaussian process maps for CVD-grown monolayer hBN. (a) 3D scatter plot of CVD-grown monolayer hBN with different recipe conditions. (b–d) Contour plots of Gaussian process regression on two-parameter space: (b) borazine flow rate vs hydrogen flow rate, (c) hydrogen flow rate vs growth temperature, and (d) borazine flow rate vs growth temperature. The coded color indicates the expected domain size of hBN. The arrows and widths of the orange lines represent the directions and the strength of the gradients, respectively. The solid green lines represent the precursor effects while the dashed green lines indicate the temperature effects.

Cu, increased desorption of N atoms compared to their lateral diffusion on the Cu surface, or even the increased desorption of the borazine precursor itself at higher temperatures.[24]

Figure 3c shows the plot of the hBN domain sizes with different flow rates of hydrogen gas in the range 1 to 100 sccm (Figure S5f–j). The flake size significantly increases with increasing the hydrogen flow rate to 40 sccm and then gradually decreases with higher hydrogen flow rates. Hydrogen plays important roles in hBN synthesis, such as being the carrier gas of hBN, diluting the precursor, cocatalyzing the dissociation of the precursor, and etching as-grown hBN during the growth process.[2,14,25] With a flow rate of hydrogen below 40 sccm, the hydrogen radical dissociates from hydrogen molecules on the Cu surface at a high temperature, facilitating the dehydrogenation process of the borazine and leading to an increased growth rate and domain size of the hBN flakes.[2,26] At higher flow rates of hydrogen, the concentration of borazine is diluted by hydrogen, leading to slower hBN growth due to the insufficient borazine supply.[25] In addition, hydrogen can result in etching as-grown hBN on Cu (111) via the reverse reaction.[14] Therefore, the hBN flakes with high hydrogen flow rates show irregular shapes, as shown in Figure S5j. Figure 3d shows the effect of borazine flow rate during hBN growth on Cu (111). The flake size of hBN increases to 20 μm as the flow rate of borazine increases to 0.1 sccm and then decreases when the flow rate increases above 0.11 sccm (Figure S5k–p). At the flow rate of 0.115 sccm, hBN flakes are merged into a continuous film due to the increased nucleation density. We attribute the phenomenon observed in Figure 3d to the change from lack to the excess of active precursors for the hBN growth.

Figure 4a shows a three-dimensional contour plot of the experimental data obtained using different CVD parameters (as discussed above), where the coded color indicates the domain size of the hBN. As can be seen from the purple color points in Figure 4a, the hBN flakes exhibit larger domain sizes under high growth temperatures and high borazine flow rates. Hence, we set the intersection point to be the temperature of 1030 °C, the borazine flow rate of 0.085 sccm, and the hydrogen flow rate of 40 sccm. By fixing one parameter of the intersection point, we explore the three recipe spaces to further understand the correlation between the different growth parameters. Before carrying out the data analysis, we applied the Matérn52 kernel (eq 1) as the covariance function in the GP model (details in the Supporting Information). Figure S8 displays the standard deviations of the GP model where the dark blue dots are the experimentally observed data points. Figure 4b–d shows the contour maps of the mean of the

https://doi.org/10.1021/acs.nanolett.2c04624
Nano Lett. 2023, 23, 4741–4748

calculated posterior distributions, with the color profiles indicating the predicted domain size. To quantitatively evaluate the correlations between the two parameters, we measured the gradients of the contour maps and performed the stream plots in Figure 4b–d. The arrow of the streamlines in Figure 4b–d represents the steepest direction of the gradients, and the width of the streamlines indicates the steepness of the gradient. By tracking the gentlest slopes which indicates the most balanced dynamic chemical reaction for maintaining a similar domain size of hBN, we drew two types of lines to show the correlations among the parameters. The solid green lines represent the precursor effects while the dashed green lines indicate the temperature effects. In Figure 4b, the solid line shows a positive slope (Figure S9) toward the optimal point, indicating that high flow rates of borazine are used for higher flow rates of hydrogen, which is because hydrogen helps to increase the domain size of hBN crystals by etching amorphous hBN clusters. In Figure 4c, the dashed line indicates lower flow rates of hydrogen are used at higher temperatures, which is due to the increase of hydrogen dissociation at higher temperatures. On the other hand, the solid line in Figure 4c represents that the hydrogen flow rate dominates the growth results in a small temperature range of about 1030–1040 °C. Similarly, the dashed line in Figure 4d shows a positive slope, indicating a higher borazine flow rate is used at the higher temperature range. This temperature effect is due to the higher desorption rate of borazine on Cu surfaces at a higher temperature. Once again, within the temperature range between 1030 and 1040 °C, the flow rate of borazine dominates the growth results. To quantitatively compare the strength of the correlations between two parameters, we measured the widths and heights for hBN domain size above 12 μm (D_{12}) in each contour plot (Figure S10). As illustrated in Figure S10b, throughout the entirety of the D_{12} region, hydrogen exhibits a tunability range of 55 resolution units, while temperature displays a tunability confined to 19 resolution units. Thus, the sensitivity of temperature is notably higher than hydrogen. Based on the system specifications and on our prior knowledge, we discretized the parameter ranges of D_{12} into parameter sensitivities by dividing the resolution of parameters. The resolutions of the parameters in our experiments are 1 °C for temperature, 1 sccm for hydrogen, and 0.005 sccm for borazine. Therefore, the sensitivities of the parameters are calculated as shown in Figure S10, indicating that the sensitivity of the borazine is higher than the sensitivities of temperature and hydrogen in our experiments. Through this methodology, we can quantitatively evaluate the sensitivities of the parameters for the hBN growth. Finally, to validate our ML approach, we compared the contour maps with and without the optimal point in Figure S11. In Figure S11a, the contour map predicts the largest hBN domain around 1033 °C and the borazine flow of 0.109 sccm. After we added the newly observed point to the database, the new contour map (Figure S11c,e with a higher-resolution color scale) shows the largest hBN domain at 1033 °C and the borazine flow rate of 0.104 sccm. Because the distance between the predicted point from Figure S11e and the newly observed point in Figure S11d is less than the parameter resolution, the predicted point is considered the optimal point. As can be seen, the predicted point in Figure S11a is well matched with the optimal point in Figure S11c. Therefore, we can confirm that the Gaussian process is validated. The methodology making use of the Gaussian distribution can help us understand the mutual effects of two CVD parameters, allowing for a comprehensive understanding of the growth mechanisms of CVD-grown hBN compared to the typical growth mechanism investigation using a single parameter. Our approach allows us to understand the nonlinear effects with multiple parameters and evaluate their importance.

In this work, we grew monolayer hBN on single-crystalline Cu (111) substrates by LPCVD. Monolayer hBN flakes were well aligned due to epitaxial growth on single-crystalline Cu (111), and their nucleation density and flake size were controlled by reducing the borazine concentration through the three-step process. In order to understand the growth dynamics of hBN on Cu (111), we varied individual growth parameters, such as the growth temperature, the flow rate of hydrogen gas, and the flow rate of borazine separately, and observed the corresponding trend of flake size and nucleation density. The activation energy of 3.63 eV was obtained for hBN nucleation on Cu (111). Furthermore, we adopted a ML model to systematically analyze these collected data, which provided the correlation between multigrowth parameters and determined the growth window on domain size through the Gaussian process. The growth temperature had a strong correlation with borazine and hydrogen while borazine is the most sensitive parameter for growing large hBN domains. This new multidimensional approach for growth parameters based on ML will open a comprehensive understanding of the growth dynamics of various materials.

■ ASSOCIATED CONTENT

Supporting Information

The Supporting Information is available free of charge at https://pubs.acs.org/doi/10.1021/acs.nanolett.2c04624.

Conversion from polycrystalline Cu to Cu(111), monolayer hBN growth and transfer, Raman spectroscopy, X-ray photoelectron spectroscopy (XPS), scanning transmission electron microscope (STEM), Gaussian process, the shape of the closed loop in the contour map, and Figures S1–S10 (PDF)

■ AUTHOR INFORMATION

Corresponding Author

Jing Kong − *Department of Electrical Engineering and Computer Science, Massachusetts Institute of Technology, Cambridge, Massachusetts 02139, United States;* orcid.org/0000-0003-0551-1208; Email: jingkong@mit.edu

Authors

Ji-Hoon Park − *Department of Electrical Engineering and Computer Science, Massachusetts Institute of Technology, Cambridge, Massachusetts 02139, United States;* orcid.org/0000-0003-4776-5206

Ang-Yu Lu − *Department of Electrical Engineering and Computer Science, Massachusetts Institute of Technology, Cambridge, Massachusetts 02139, United States*

Mohammad Mahdi Tavakoli − *Department of Electrical Engineering and Computer Science, Massachusetts Institute of Technology, Cambridge, Massachusetts 02139, United States;* orcid.org/0000-0002-8393-6028

Na Yeon Kim − *Department of Physics and Astronomy and California NanoSystems Institute, University of California, Los Angeles, Los Angeles, California 90095, United States*

https://doi.org/10.1021/acs.nanolett.2c04624
Nano Lett. 2023, 23, 4741−4748

Ming-Hui Chiu − *Department of Electrical Engineering and Computer Science, Massachusetts Institute of Technology, Cambridge, Massachusetts 02139, United States*
Hongwei Liu − *Department of Electrical Engineering and Computer Science, Massachusetts Institute of Technology, Cambridge, Massachusetts 02139, United States; Department of Chemical and Biological Engineering, Hong Kong University of Science and Technology, Kowloon, Hong Kong 999077, China*
Tianyi Zhang − *Department of Electrical Engineering and Computer Science, Massachusetts Institute of Technology, Cambridge, Massachusetts 02139, United States;* orcid.org/0000-0002-8998-3837
Zhien Wang − *Department of Electrical Engineering and Computer Science, Massachusetts Institute of Technology, Cambridge, Massachusetts 02139, United States*
Jiangtao Wang − *Department of Electrical Engineering and Computer Science, Massachusetts Institute of Technology, Cambridge, Massachusetts 02139, United States;* orcid.org/0000-0001-7323-4690
Luiz Gustavo Pimenta Martins − *Physics Department, Massachusetts Institute of Technology, Cambridge, Massachusetts 02139, United States;* orcid.org/0000-0001-9777-7999
Zhengtang Luo − *Department of Chemical and Biological Engineering, Hong Kong University of Science and Technology, Kowloon, Hong Kong 999077, China;* orcid.org/0000-0002-5134-9240
Miaofang Chi − *Center for Nanophase Materials Sciences, Oak Ridge National Laboratory, Oak Ridge, Tennessee 37831, United States;* orcid.org/0000-0003-0764-1567
Jianwei Miao − *Department of Physics and Astronomy and California NanoSystems Institute, University of California, Los Angeles, Los Angeles, California 90095, United States*

Complete contact information is available at: https://pubs.acs.org/10.1021/acs.nanolett.2c04624

Author Contributions

J.-H.P. and A.-Y.L. contributed equally to this work. The manuscript was written through contributions of all authors. All authors have given approval to the final version of the manuscript.

Notes

The authors declare no competing financial interest.

■ ACKNOWLEDGMENTS

J.-H.P., A.-Y.L., J.W., and J.K. acknowledge the support from the U.S. Army Research Office (ARO) MURI project under grant W911NF-18-1-04320431 and the US Army Research Office through the Institute for Soldier Nanotechnologies at MIT, under cooperative agreement W911NF-18-2-0048. T.Z., Z.W., and J.K. acknowledge the support from the U.S. Department of Energy (DOE), Office of Science, Basic Energy Sciences (BES) under award DE-SC0020042. J.M. acknowledges partial support by the US Department of Energy (DOE), Office of Science, Basic Energy Sciences (BES), Division of Materials Sciences and Engineering, under award DE-SC0010378. The STEM experiment was performed at the Center for Nanophase Materials Sciences (CNMS), which is a U.S. Department of Energy Office of Science User Facility. M.C. acknowledges Early Career project FWP# ERKCZ55 supported by the DOE Office of Science.

■ REFERENCES

(1) Watanabe, K.; Taniguchi, T.; Kanda, H. Direct-Bandgap Properties and Evidence for Ultraviolet Lasing of Hexagonal Boron Nitride Single Crystal. *Nat. Mater.* **2004**, *3* (6), 404−409.
(2) Lee, J. S.; Choi, S. H.; Yun, S. J.; Kim, Y. I.; Boandoh, S.; Park, J.-H.; Shin, B. G.; Ko, H.; Lee, S. H.; Kim, Y.-M.; Lee, Y. H.; Kim, K. K.; Kim, S. M. Wafer-Scale Single-Crystal Hexagonal Boron Nitride Film via Self-Collimated Grain Formation. *Science* **2018**, *362* (6416), 817−821.
(3) Mogg, L.; Zhang, S.; Hao, G.-P.; Gopinadhan, K.; Barry, D.; Liu, B. L.; Cheng, H. M.; Geim, A. K.; Lozada-Hidalgo, M. Perfect Proton Selectivity in Ion Transport through Two-Dimensional Crystals. *Nat. Commun.* **2019**, *10* (1), 4243.
(4) Tavakoli, M. M.; Park, J.; Mwaura, J.; Saravanapavanantham, M.; Bulović, V.; Kong, J. Monolayer Hexagonal Boron Nitride: An Efficient Electron Blocking Layer in Organic Photovoltaics. *Adv. Funct. Mater.* **2021**, *31*, 2101238.
(5) Chen, S.; Zhu, C.; Gu, H.; Wang, L.; Qi, J.; Zhong, L.; Zhang, Z.; Yang, C.; Shi, G.; Zhao, S.; Li, S.; Liu, K.; Zhang, L. Enhanced Electrochemical Methanation of Carbon Dioxide at the Single-Layer Hexagonal Boron Nitride/Cu Interfacial Perimeter. *Nano Lett.* **2021**, *21* (10), 4469−4476.
(6) Xu, X.; Zhang, Z.; Dong, J.; Yi, D.; Niu, J.; Wu, M.; Lin, L.; Yin, R.; Li, M.; Zhou, J.; Wang, S.; Sun, J.; Duan, X.; Gao, P.; Jiang, Y.; Wu, X.; Peng, H.; Ruoff, R. S.; Liu, Z.; Yu, D.; Wang, E.; Ding, F.; Liu, K. Ultrafast Epitaxial Growth of Metre-Sized Single-Crystal Graphene on Industrial Cu Foil. *Science Bulletin.* **2017**, *62*, 1074−1080.
(7) Jin, S.; Huang, M.; Kwon, Y.; Zhang, L.; Li, B.-W.; Oh, S.; Dong, J.; Luo, D.; Biswal, M.; Cunning, B. V.; Bakharev, P. V.; Moon, I.; Yoo, W. J.; Camacho-Mojica, D. C.; Kim, Y.-J.; Lee, S. H.; Wang, B.; Seong, W. K.; Saxena, M.; Ding, F.; Shin, H.-J.; Ruoff, R. S. Colossal Grain Growth Yields Single-Crystal Metal Foils by Contact-Free Annealing. *Science* **2018**, *362* (6418), 1021−1025.
(8) Wu, M.; Zhang, Z.; Xu, X.; Zhang, Z.; Duan, Y.; Dong, J.; Qiao, R.; You, S.; Wang, L.; Qi, J.; Zou, D.; Shang, N.; Yang, Y.; Li, H.; Zhu, L.; Sun, J.; Yu, H.; Gao, P.; Bai, X.; Jiang, Y.; Wang, Z.-J.; Ding, F.; Yu, D.; Wang, E.; Liu, K. Seeded Growth of Large Single-Crystal Copper Foils with High-Index Facets. *Nature* **2020**, *581* (7809), 406−410.
(9) Wang, L.; Xu, X.; Zhang, L.; Qiao, R.; Wu, M.; Wang, Z.; Zhang, S.; Liang, J.; Zhang, Z.; Zhang, Z.; Chen, W.; Xie, X.; Zong, J.; Shan, Y.; Guo, Y.; Willinger, M.; Wu, H.; Li, Q.; Wang, W.; Gao, P.; Wu, S.; Zhang, Y.; Jiang, Y.; Yu, D.; Wang, E.; Bai, X.; Wang, Z.-J.; Ding, F.; Liu, K. Epitaxial Growth of a 100-Square-Centimetre Single-Crystal Hexagonal Boron Nitride Monolayer on Copper. *Nature* **2019**, *570* (7759), 91−95.
(10) Chen, T.-A.; Chuu, C.-P.; Tseng, C.-C.; Wen, C.-K.; Wong, H.-S. P.; Pan, S.; Li, R.; Chao, T.-A.; Chueh, W.-C.; Zhang, Y.; Fu, Q.; Yakobson, B. I.; Chang, W.-H.; Li, L.-J. Wafer-Scale Single-Crystal Hexagonal Boron Nitride Monolayers on Cu (111). *Nature* **2020**, *579* (7798), 219−223.
(11) Song, X.; Gao, J.; Nie, Y.; Gao, T.; Sun, J.; Ma, D.; Li, Q.; Chen, Y.; Jin, C.; Bachmatiuk, A.; Rümmeli, M. H.; Ding, F.; Zhang, Y.; Liu, Z. Chemical Vapor Deposition Growth of Large-Scale Hexagonal Boron Nitride with Controllable Orientation. *Nano Research.* **2015**, *8*, 3164−3176.
(12) Stehle, Y.; Meyer, H. M., III; Unocic, R. R.; Kidder, M.; Polizos, G.; Datskos, P. G.; Jackson, R.; Smirnov, S. N.; Vlassiouk, I. V. Synthesis of Hexagonal Boron Nitride Monolayer: Control of Nucleation and Crystal Morphology. *Chem. Mater.* **2015**, *27* (23), 8041−8047.
(13) Tay, R. Y.; Wang, X.; Tsang, S. H.; Loh, G. C.; Singh, R. S.; Li, H.; Mallick, G.; Teo, E. H. T. A Systematic Study of the Atmospheric Pressure Growth of Large-Area Hexagonal Crystalline Boron Nitride Film. *J. Mater. Chem. C* **2014**, *2*, 1650.
(14) Wang, L.; Wu, B.; Jiang, L.; Chen, J.; Li, Y.; Guo, W.; Hu, P.; Liu, Y. Growth and Etching of Monolayer Hexagonal Boron Nitride. *Adv. Mater.* **2015**, *27* (33), 4858−4864.

(15) Jang, S. K.; Youn, J.; Song, Y. J.; Lee, S. Synthesis and Characterization of Hexagonal Boron Nitride as a Gate Dielectric. *Sci. Rep.* **2016**, *6*, 30449.
(16) Park, J.-H.; Lu, A.-Y.; Shen, P.-C.; Shin, B. G.; Wang, H.; Mao, N.; Xu, R.; Jung, S. J.; Ham, D.; Kern, K.; Han, Y.; Kong, J. Synthesis of High-Performance Monolayer Molybdenum Disulfide at Low Temperature. *Small Methods* **2021**, *5* (6), e2000720.
(17) Liu, S.; van Duin, A. C. T.; van Duin, D. M.; Liu, B.; Edgar, J. H. Atomistic Insights into Nucleation and Formation of Hexagonal Boron Nitride on Nickel from First-Principles-Based Reactive Molecular Dynamics Simulations. *ACS Nano* **2017**, *11* (4), 3585−3596.
(18) Rasmussen, C. E.; Williams, C. K. I. *Gaussian Processes for Machine Learning*; MIT Press: 2005; pp 1−104.
(19) Park, J.-H.; Park, J. C.; Yun, S. J.; Kim, H.; Luong, D. H.; Kim, S. M.; Choi, S. H.; Yang, W.; Kong, J.; Kim, K. K.; Lee, Y. H. Large-Area Monolayer Hexagonal Boron Nitride on Pt Foil. *ACS Nano* **2014**, *8* (8), 8520−8528.
(20) Chen, S.; Ji, H.; Chou, H.; Li, Q.; Li, H.; Suk, J. W.; Piner, R.; Liao, L.; Cai, W.; Ruoff, R. S. Millimeter-Size Single-Crystal Graphene by Suppressing Evaporative Loss of Cu during Low Pressure Chemical Vapor Deposition. *Adv. Mater.* **2013**, *25* (14), 2062−2065.
(21) Hsieh, Y.-P.; Chen, D.-R.; Chiang, W.-Y.; Chen, K.-J.; Hofmann, M. Recrystallization of Copper at a Solid Interface for Improved CVD Graphene Growth. *RSC Advances.* **2017**, *7*, 3736−3740.
(22) Gorbachev, R. V.; Riaz, I.; Nair, R. R.; Jalil, R.; Britnell, L.; Belle, B. D.; Hill, E. W.; Novoselov, K. S.; Watanabe, K.; Taniguchi, T.; Geim, A. K.; Blake, P. Hunting for Monolayer Boron Nitride: Optical and Raman Signatures. *Small* **2011**, *7* (4), 465−468.
(23) Ohring, M. *The Materials Science of Thin Films*; Academic Press: 1992; pp 357−415.
(24) Kidambi, P. R.; Blume, R.; Kling, J.; Wagner, J. B.; Baehtz, C.; Weatherup, R. S.; Schloegl, R.; Bayer, B. C.; Hofmann, S. In Situ Observations during Chemical Vapor Deposition of Hexagonal Boron Nitride on Polycrystalline Copper. *Chem. Mater.* **2014**, *26* (22), 6380−6392.
(25) Wu, Q.; Park, J.-H.; Park, S.; Jung, S. J.; Suh, H.; Park, N.; Wongwiriyapan, W.; Lee, S.; Lee, Y. H.; Song, Y. J. Single Crystalline Film of Hexagonal Boron Nitride Atomic Monolayer by Controlling Nucleation Seeds and Domains. *Sci. Rep.* **2015**, *5*, 16159.
(26) Koepke, J. C.; Wood, J. D.; Chen, Y.; Schmucker, S. W.; Liu, X.; Chang, N. N.; Nienhaus, L.; Do, J. W.; Carrion, E. A.; Hewaparakrama, J.; Rangarajan, A.; Datye, I.; Mehta, R.; Haasch, R. T.; Gruebele, M.; Girolami, G. S.; Pop, E.; Lyding, J. W. Role of Pressure in the Growth of Hexagonal Boron Nitride Thin Films from Ammonia-Borane. *Chem. Mater.* **2016**, *28*, 4169−4179.

https://doi.org/10.1021/acs.nanolett.2c04624
Nano Lett. 2023, 23, 4741−4748